Chapter 10
Dynamic Modeling of an Asbestos Removal Mobile Manipulator for Stability Evaluation

Siddharth Maraje, Chedli-Belhassen Bouzgarrou, Jean-Christophe Fauroux, and Lounis Adouane

The H2020 project Ro**bots to Rec**onstruction [3] was started with an aim to bring automation into the construction industry. A general concept of the robotized asbestos removal process is illustrated in Fig. 10.1. Multiple semi-autonomous robotic units equipped with the grinding tool are deployed in the cleaning environment. They also possess asbestos detectors which provide input to the mobile base localization. The local process monitoring then controls the grinding process through tool path planning. The two prototypes developed during the project are shown in Fig. 10.2. The version-1 prototype has 6 caster wheels in total. The two central wheels are the drive wheels while the four corner wheels stay non actuated. The version-2 prototype however has four Swedish wheels. The two versions also differ in terms of the arm architecture integrated into them. Version-1 is added with the P-6R arm while version-2 has 7R architecture.

This chapter presents an extract of the work done by authors during the course of the project. Initially, the state of the art consisting of a variety of stability indices (margins) relevant to mobile manipulators is presented. Thereafter, dynamic modeling of the asbestos removal environment and the use-case in different cleaning scenarios is shown. Two methods of stability evaluation are then demonstrated in detail and an example of zig-zag tool trajectory.

S. Maraje · C.-B. Bouzgarrou (✉) · J.-C. Fauroux · L. Adouane
Universitä Clermont Auvergne, CNRS, Clermont Auvergne INP, Institut Pascal,
Clermont-Ferrand 63000, France
e-mail: belhassen-chedli.bouzgarrou@sigma-clermont.fr

L. Adouane
Universitä de technologie de Compiägne (UTC), CNRS, Heudiasyc, Compiägne 60200, France
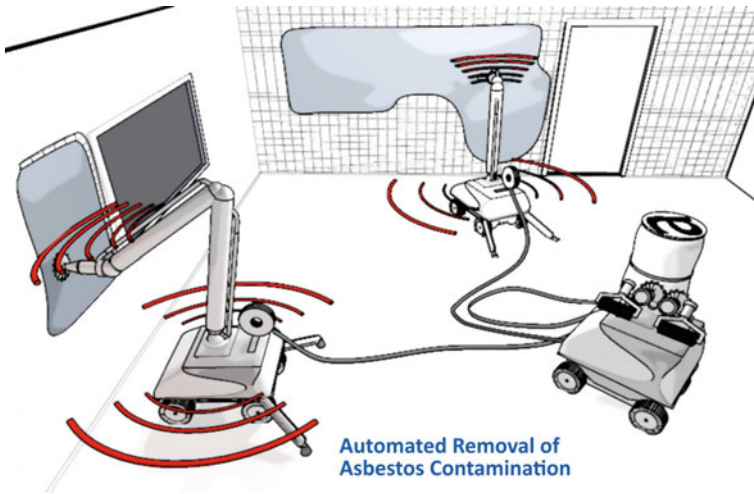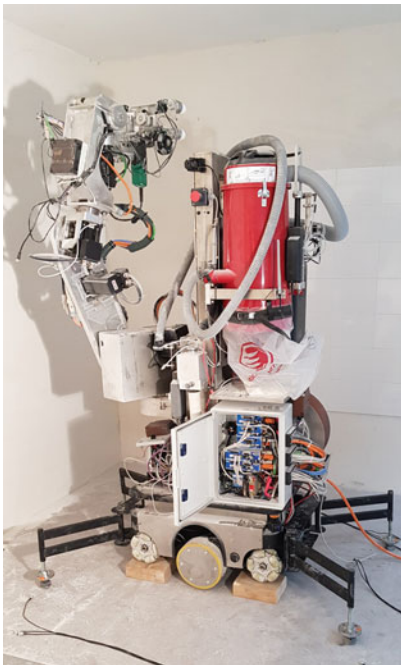
Fig. 10.1 The concept of robotized asbestos removal process [3]

(a) Prototype version-1   (b) Prototype version-2

Fig. 10.2 Two prototypes developed by the consortium of Bots2ReC

10.1 Stability Indices for Mobile Manipulators

For mobile manipulators and robots in general, including wheeled and legged ones, numerous attempts to accurately evaluate stability can be seen through the literature. A condition to determine the state of stability or instability is called a *criterion*, while a quantitative measure of stability is termed as *margin*. A review of static and dynamic margins was presented in [2]. In [12], based on stability metric, criteria were further classified into five types namely: distance, angle, force, moment and energy. This classification is adapted for presenting the state of the art through the following sections.

10.1.1 Distance Based Indices

Distance-based criteria use the minimum distance between the projection of the centre of gravity on the support polygon C.G and an edge of the support polygon to define instantaneous stability. In [13] and [14], a static stability criterion based on the C.G was proposed. The claim was, a vehicle (wheeled or legged) is statically stable if '*the projection of its centre of mass lies within the supporting polygon*'. Support polygon of the footprint of the robot was defined as a convex polygon formed by connecting ground-wheel contact points.

Figures 10.3 and 10.4 respectively show statically stable and unstable poses of the mobile manipulator. Rectangular support polygon of the mobile manipulator defined by points $S_{11}S_{12}S_{21}S_{22}$.

Sreenivasan [21] proposed a distance-based dynamic stability margin (Fig. 10.5). It projected the dynamic force F_g applied on the C.G of the robot to the ground and measured the distance d between the line of action of the force and a parallel line

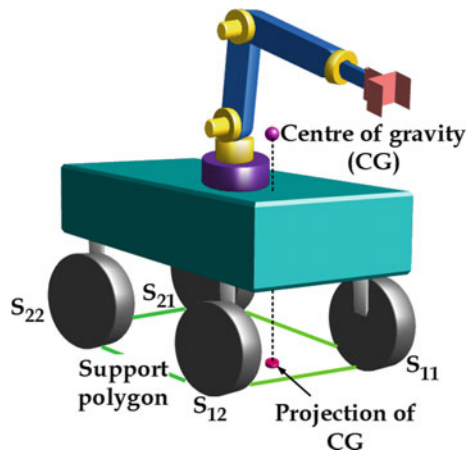**Fig. 10.3** Statically stable pose
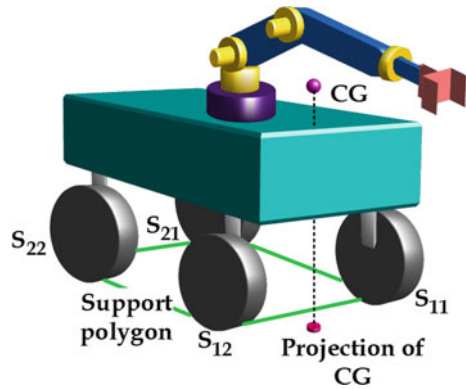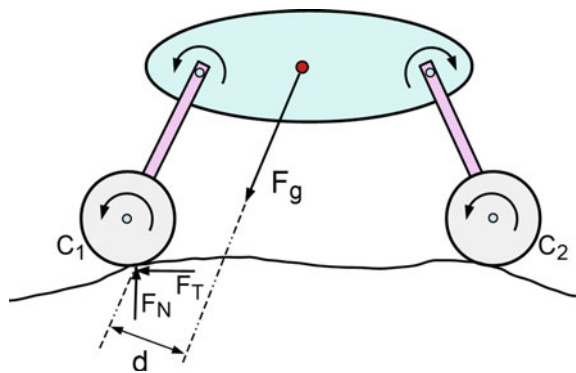
Fig. 10.4 Statically unstable pose

Fig. 10.5 Distance based dynamic stability margin [21]

passing through ground contact point. But this margin had a limitation of not being able to handle dynamic toques applied on the mobile platform.

Davidson and Schweitzer [4] proposed a static stability margin for four-legged robots. In their method, external forces, the force from a tethering cable-winch and inertial force were included in a quasi-static manner as a wrench. Possible rotation of the vehicle around the axis defined by each edge of the support polygon is defined as a twist of zero pitch. Virtual power generated by a resultant wrench and zero-pitch virtual twist was determined for all edges of the support polygon. A negative value of virtual power was identified as a condition of instability. The minimum magnitude of this power was used as a value for stability margin.

10.1.2 Angle Based Indices

In [5], subtended angle (θ) between normal of the ith tip-over axis and ith resultant force is considered as a measure of stability about ith tip-over axis. The minimum of all such angles calculated for respective axes is the stability margin of the entire system.
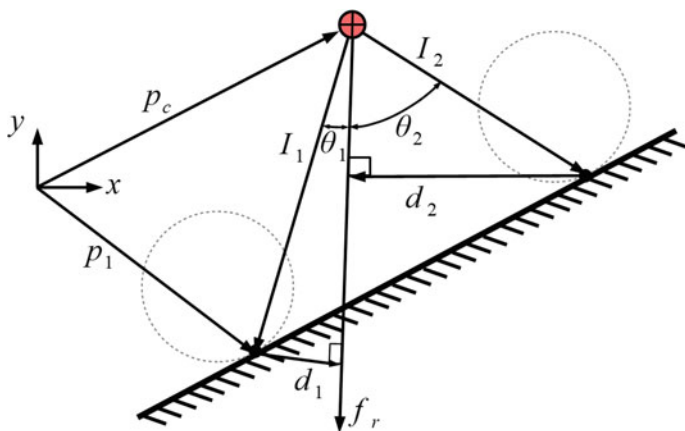
Fig. 10.6 Concept of force angle stability margin [19]

$$\theta = min(\theta_i) \tag{10.1a}$$

$$\theta > 0 \rightarrow stable; \quad \theta = 0 \rightarrow marginally\ stable; \quad \theta < 0 \rightarrow unstable \tag{10.1b}$$

Another tip-over stability margin called force-angle stability measure (FASM) was proposed in [19]. The claim was an easy calculation and sensitivity to top-heaviness. According to the author—'force-angle stability measure is based on the computation of *minimum of the angle between the net force vector and a normal to each of the tip-over axis* (Fig. 10.6)'.

$$\beta = \theta_i.||d_i||.||f_r|| \tag{10.2}$$

Critical tipover instability occurs when β goes to zero, i.e., any θ_i becomes zero, or either of $||d_i||$ or the force f_r become zero.

10.1.3   Energy Based Indices

Messuri and Klein [15] proposed **energy stability margin** (ESM) as an improvement to the static stability margin. Energy stability level associated with a particular edge of a support polygon is equal to the mechanical work required to rotate the body centre of gravity about an edge to a position where the vertical projection of CG lies along that edge of the support polygon (to the verge of instability). The energy stability margin is equal to the minimum of the energy stability levels associated with all the edges of the support polygon.
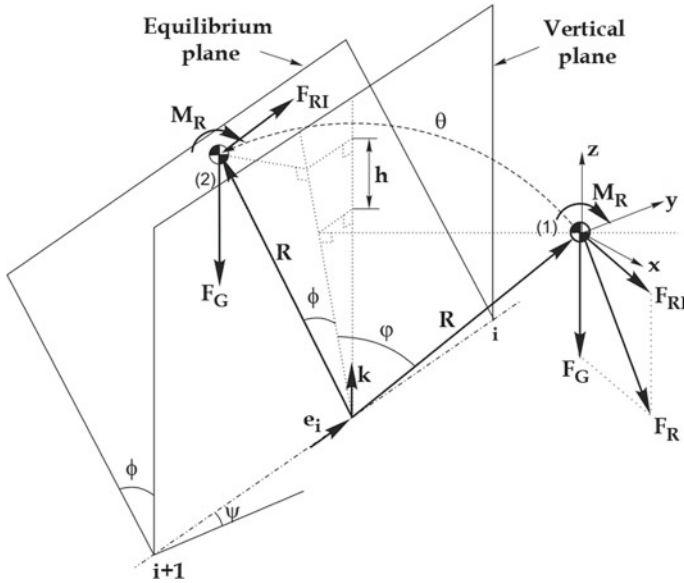
Fig. 10.7 Equilibrium plane corresponding to the tip-over edge, [8, 9]

$$S_{ESM} = \min_{i=1}^{n_s}(mgh_i) \tag{10.3}$$

'i' is a vertex of the support polygon which form a rotational axis with $i + 1$, n_s is the number of supporting legs and h_i is the elevation of C.G during the tip-over process (Fig. 10.7).

Ghasempoor and Sepehri [8] extended ESM for mobile manipulators by including other factors affecting stability—vehicle top-heaviness, uneven terrain conditions, external forces arising from the manipulation of payload and inertial forces due to vehicle motions. ESM is intended to monitor the tip-over potential of mobile manipulators. An *equilibrium plane* (π_s) associated with each edge of the support polygon was defined such that, the plane contains the centre of gravity at the hypothetical tilted position of the mobile manipulator system for which projection of the centre of gravity on p_S is on the respective edge. Figure 10.8 shows the hypothetical tip-over of the mobile robotic system. For this state of tilt, the projection of the centre of gravity lies on the edge S_{11}–S_{22}. The equilibrium plane denoted by π_s is thus defined to pass through edge S_{11}–S_{22} and centre of gravity.

The energy stability level associated with each edge was defined as the mechanical work required to rotate the system about the respective edge till the centre of gravity lies in the equilibrium plane. The minimum of all the energy levels was regarded as a dynamic energy stability margin (DESM). Energy associated with the supporting edge defined by points (i)–$(i + 1)$ was calculated as,
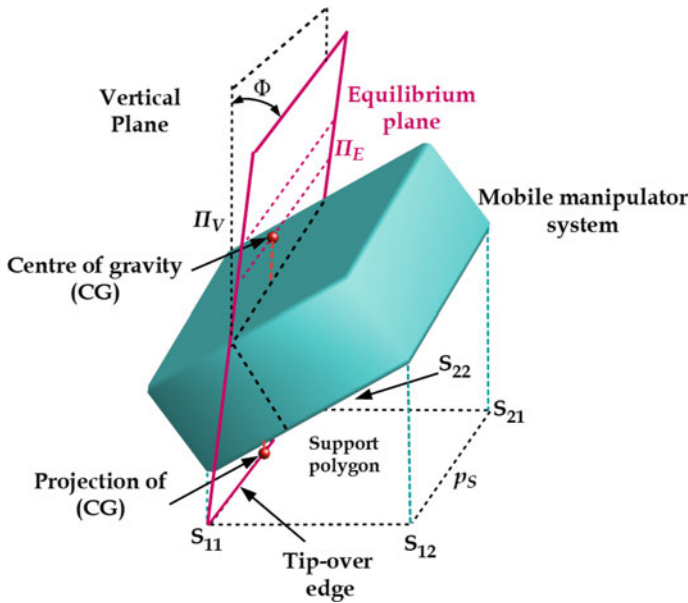
Fig. 10.8 Hypothetical tipover of the robotic system

$$Energy\ Stability\ Level_{(i,i+1)} = [W_1 - W_2]_{(i,i+1)}; \tag{10.4}$$

Here, W_1 is work done by stabilizing weight force and W_2 is work done by destabilizing forces and moments.

In [9] normalized energy stability margin was proposed as the difference between the initial position of the center of gravity and its highest position in the process of tumbling.

$$S_{NESM} = \frac{S_{ESM}}{mg} = \min_{i=1}^{n_s}(h_i) \tag{10.5}$$

Here, the n_s is the number of edges of the support polygon, and h_i is the elevation of the height of the C.G during tip-over. In [7] this concept was extended to walking machines considering leg dynamic effect a disturbance. It was stated that a walking machine is dynamically stable if every moment M_i around the edge i of the support polygon due to robot/ground forces moments is positive. The positive direction was the clockwise direction of the force around the support polygon. Energy stability level for all the edges was calculated as a *difference of potential and kinetic energy*. Thus, the **normalised energy stability margin** (S_{NEDSM}) was defined as:

$$S_{NEDSM} = \frac{min(E_i)}{mg} \tag{10.6}$$

10.1.4 Moment Based Indices

Dynamic stability margin was proposed in [11] as the smallest of all moments M_i around the edges of the support polygon. This margin considered robot/ground interaction forces and was normalized by the weight of the system.

$$S_{DSM} = \min_{i=1}^{n} \frac{e_i . (F_R \times P_i + M_R)}{mg} \tag{10.7}$$

Yoneda and Hirose [24] presented tumble stability criterion and introduced a counter-force limit as an index to indicate manipulation capabilities. The concept of stability is based on the ability of virtually lost wheel-ground contact points to generate support force required to suppress tumbling. Mathematical expression to calculate this margin is:

$$Tumble\ \ stability\ \ margin = \frac{min \left| \bar{M}.\frac{(p_a - p_b)}{|p_a - p_b|} + \bar{F}.\frac{(p_b \times p_a)}{|p_a - p_b|} \right|}{mg} \tag{10.8}$$

Here, $\bar{M}$ and $\bar{F}$ are net moment and force acting at CG, p_a and p_b are the coordinate vectors of the adjacent ground contact points that define axis of rotation.

Sugano et al. [22] was one of the initial works to introduce zero moment point (ZMP) as a stability criteria for mobile manipulators. It was identified that the stability of a mobile manipulator is closely related to the motion of the mobile base, posture and motion of the onboard manipulator and external forces on the end-effector. Based on ZMP, two concepts named *stability degree* and *valid stable region* are proposed. The former defined the stable limit while the later was used to discuss the influence of disturbances in the task environment.

In this chapter, the support polygon of the mobile manipulator system was called *stable region*. A maximal stability curve (which is a straight line) was identified inside the stable region such that, stability is highest when ZMP lies on this curve. To ensure the safety of the mobile manipulator under the influence of external forces or environmental disturbances, a valid stable region was defined such that, if ZMP lies within this region, stability is ensured. i.e. ZMP lies within the stable region (support polygon) after being displaced (Fig. 10.9).

In [16, 17] Moment Height Tip-over Measure (MHS) was proposed. This index was proved to be computationally less expensive than energy and force-based margins. The resultant of force and moments exerted by the manipulator on the mobile base was calculated. Then the moment of this resultant about corner points of the support polygon was found. These moments were then projected on the respective edges of the support polygon. To make the criterion sensitive to the height of the CG, a multiplicative term h_{cm} was added to the MHS. In order to calculate the MHS, requirements are: all joint angles, velocities and accelerations of onboard manipulator, linear and angular accelerations of a mobile base, knowledge of external forces and torques exerted on the system.
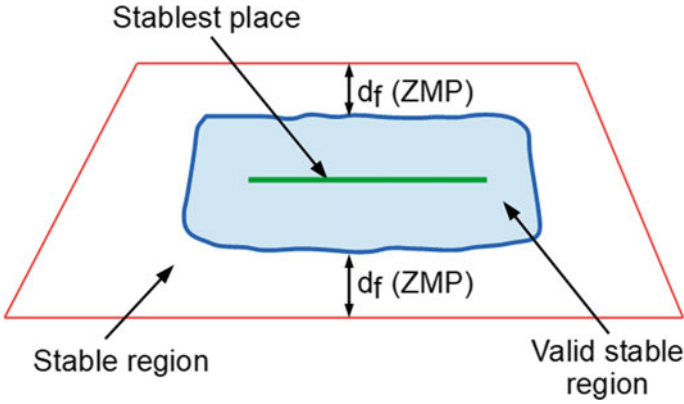
Fig. 10.9 Concept of stable and valid stable region [22]

MHS measure α is computed in (10.9),

$$\alpha = \min_i(\alpha_i) \quad i = \{1, 2, 3, 4...\} \tag{10.9}$$

Here, α_i denotes dynamic MHS measure about ith edge which is given as,

$$\alpha_i = (I_i)^\sigma M_i \tag{10.10}$$

Here, I_i is the moment of inertia of mobile base about ith axis, M_i is moment about ith axis and $\sigma = 1$ if $M_i > 0$ else -1.

Roan et al. [20] presented a real-world validation of three tip-over algorithms: Zero-Moment point (ZMP), Force-Angle stability measure (FA) and Moment-Height Stability (MHS). A scoring scheme was implemented to record values of criteria at the actual time of tip-over, to record lag/lead of criteria and to count false positives. FA and MHS are found to be quite identical except for negative values.

Lee et al. [10] proposed the concept of a modified zero moment point for evaluating tip-over of mobile robots over uneven terrain. The turnover stability index for linear acceleration and rotational velocity are defined with the modified ZMP. The turnover stability space (TSS) with turnover stability indices is presented to control the mobile robot in order to avoid turnover effectively.

10.1.5 Force Based Indices

Mahdi and Nestinger [12] proposed a foot force criterion as an attempt to provide a quantitative measure to determine how far away the robot is from either instability or from the maximum stable pose. Mathematically foot force stability criterion is expressed as
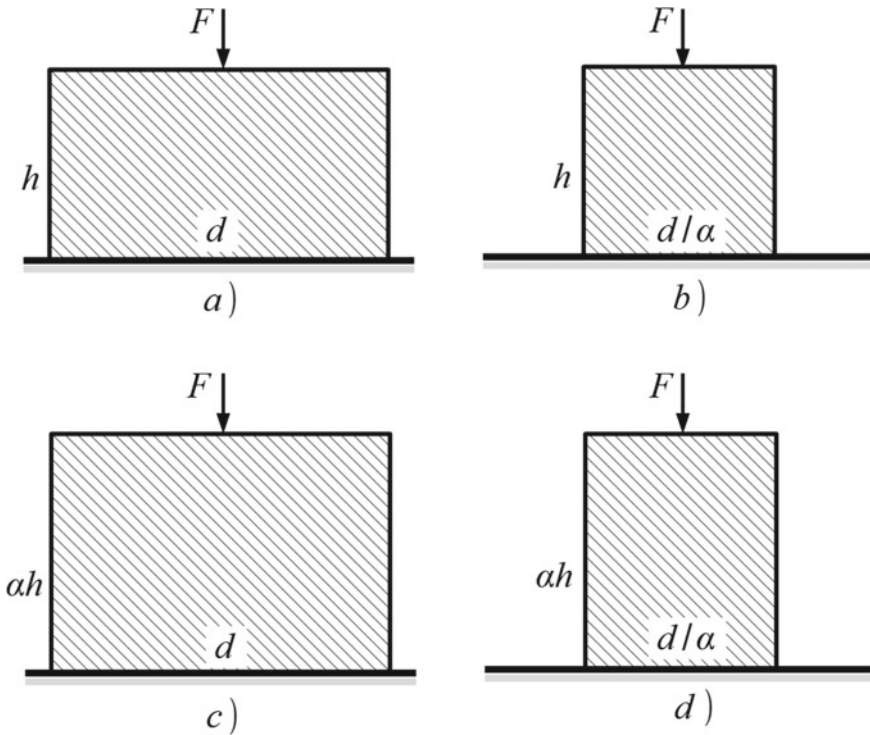
Fig. 10.10 Effect of top-heaviness on stability [12]

$$FFSM = \frac{f_1 f_2 \cdots f_n}{\bar{f}^n} \qquad 0 \leq FFSM \leq 1 \qquad (10.11)$$

Here, n is the number of supporting legs with strictly positive foot force, f_i is the magnitude of ith normal foot force and $\bar{f} = \frac{1}{n} \sum_{1=1}^{n} f_i$. An important feature of the stability margins that are based on foot forces that all the effects of gravity, external forces, inertial forces and disturbances are reflected in foot forces [18].

Figure 10.10 presents cross-sections of four different mobile bases with different aspect ratios. Considering lateral disturbances, these systems differ in terms of tip-over potential: Fig. 10.10a has the highest while Fig. 10.10d has the lowest geometric tip-over potential. Depending on the magnitude of the force F, the potential changes for all cases. This is defined as a sensitivity to top-heaviness.

Modified foot force stability margin is given by following equation:

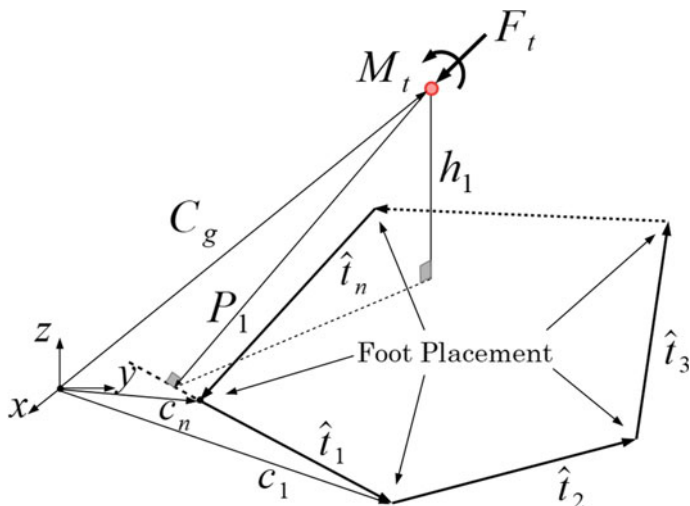$$MFFSM = FFSM. \frac{(P_i)^j}{h_i}.f \qquad (10.12)$$

Fig. 10.11   Schematic of general n-legged robot [12]

Here, $j = 1$ if the projection of CG is inside support polygon else, 0. h_i is the height of the CG with respect to tip-over the axis and P_i is tip-over axis normal as shown in Fig. 10.11.

Ding et al. [6] presented an improved tip-over moment stability criterion taking into account wheel-ground and vehicle-manipulator interaction. Based on this criterion a real-time tip-over avoidance algorithm was proposed to minimize the tip-over moment transfer. It used two sets of corrective actions: adjusting the posture of the onboard manipulator or changing the running velocity of the vehicle.

10.2   Dynamic Modeling of the Asbestos Removal Environment

The dynamic nature of the asbestos removal process generates the need for setting up a simulation model for assessing the behaviour of the robotic unit while performing removal operation. The primary objective of this assessment is stability evaluation of the robotic unit to ensure safe and stable operation. In this context, the chapter presents a methodology adapted to study the dynamic behaviour of the robotic unit. Initially, the environment to be cleaned and its key components are presented. Thereafter, cleaning scenarios arising due to the presence of different entities like wall, ceiling and ground are analysed to identify the reaction wrench and its effect on the stability of the robotic unit. Finally, two methods of stability evaluation, MATLAB-numerical and ADAMS-MATLAB co-simulation are explained in detail.
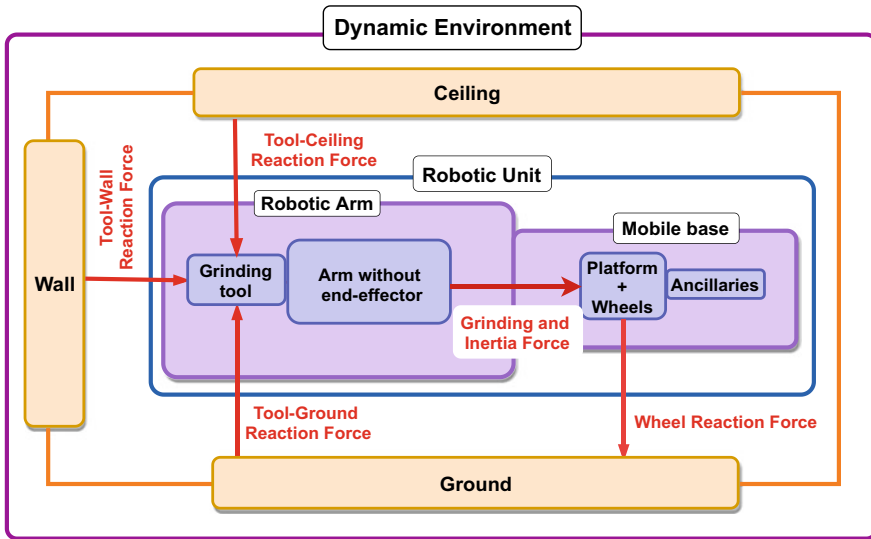
Fig. 10.12 Interaction model of asbestos removal use case

10.2.1 Need of Dynamic Modeling

The process of asbestos removal involves dynamic interaction between the cleaning environment and the robotic unit. This interaction occurs at two levels. Firstly, a grinding tool mounted on the robotic arm interacts with the cleaning surface and generate reaction forces. Secondly, wheels of the mobile base are subjected to ground reaction forces due to:

- weight of the robotic unit
- grinding forces (normal and tangential reaction forces, three reaction wrenches)
- inertia forces generated due to the motion of robotic arm and tool rotation.

In Fig. 10.12 a typical interaction model existing within the process of asbestos removal is detailed. Reaction forces generated by tool-surface interaction (ground, wall and ceiling) are transmitted to the arm through tool-arm connection. Since, arm performs accelerated motions, varying inertial forces are generated in addition to the grinding reaction forces. The connection of the arm to the mobile base transmits these forces to the mobile base which are further passed on to the ground surface through wheels. Due to these transmissions, stability of the robotic unit is significantly affected. Therefore, in order to study the effects of arm motion and grinding reaction forces on the stability of robotic unit, a dynamic simulation model capable of simulating a realistic asbestos removal scenario must be constructed.

For realistic simulation of the process, intended dynamic model should incorporate following components:

- Cleaning environment consisting of elements like wall, ground and ceiling.
- Multi-body dynamic model of the robotic unit localized inside cleaning environment (with inertial parameters: mass, centre of mass, inertia).
- Geometric and kinematic models (direct and inverse) of the robotic arm for motion generation.
- Tool-wall and wheel-ground contacts to simulate robot-environment dynamic interaction.
- Control scheme to govern the motion of the robotic arm.
- Formulation for dynamic stability of the robotic unit.

In the following sections, components of dynamic model are explained in detail.

10.2.2 Cleaning Environment

A cleaning environment is typically a rehabilitation site located in a residency building. The site consists of rooms like a bedroom, office/study room, living room, kitchen, dining room, front entrance, garden, laundry room, etc. They vary in terms of dimensions (ceiling height, room width and length) as well as materials used for construction (resurfacing concrete, plaster, bricks, tiles etc.). However, one obvious commonality for all the rooms is that the surfaces to clean can be on the ground, the walls or the ceiling.

10.2.3 Description of Representative Frames

To represent the environment as well as the robotic unit, coordinate frames are defined for individual entities (Fig. 10.13). Here, we consider the surfaces of the room are perfectly planar and perpendicular to each other. Also, an important assumption for the placement of the robotic unit throughout the cleaning operation is to have a longitudinal axis of the robotic unit perpendicular to the frontal wall. Let, **w** and **h** be the width and the height vectors of the frontal wall. The frames consist of three mutually perpendicular unit vectors. A detailed description of these frames goes below:

Environment frame ($\mathcal{F}_\mathcal{E}$) Environment mainly consists of three surfaces i.e. wall, ceiling and ground. In most of the cases where walls are planar (i.e. without curvatures), these three surfaces can help to define the global environment frame of reference. The origin of the frame is named as O_E. Position of O_E can be assumed at a convenient location e.g. centre of the room, corner of the room etc. Axis $\mathbf{x_E}$ is defined as normal to plane $\mathrm{P_W}$ point inside the room. Then, axes $\mathbf{x_E}$ and $\mathbf{y_E}$ can be
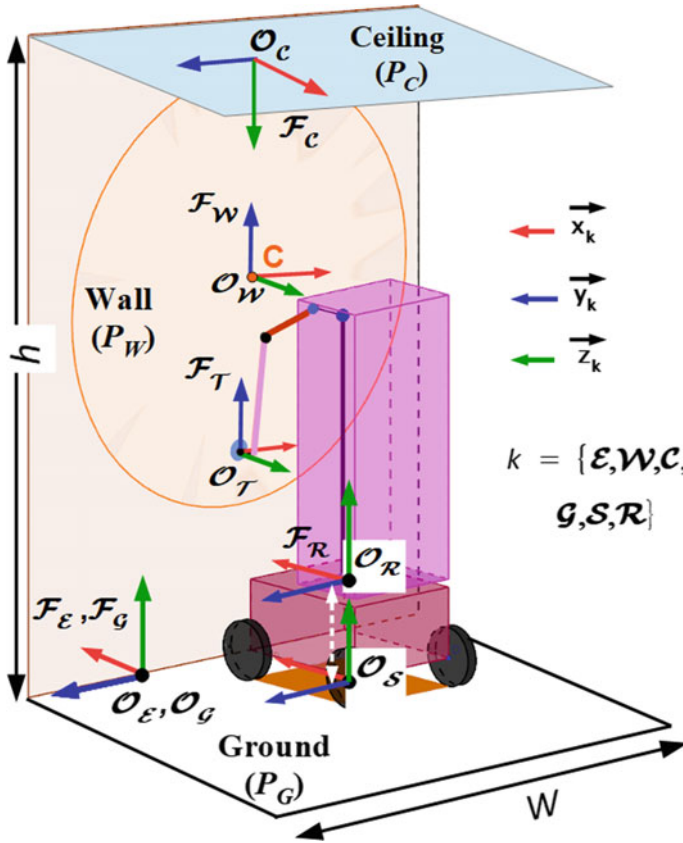
Fig. 10.13 Description of cleaning environment and frames

defined as mutually perpendicular axes that lie in the ground plane P_W. Axis y_E is selected along the line of intersection of planes P_W and P_G and its direction is shown in Fig. 10.13. According to general conventions, $\mathbf{x_E} = \mathbf{y_E} \times \mathbf{z_E}$.

Ground frame ($\mathcal{F}_G$) Ground frame $\mathcal{F}_G$ is assumed to be oriented parallel to the frame $\mathcal{F}_E$. So the axis $\mathbf{z_E}$ is normal to the plane P_G. Position of the origin O_G can be assumed at any convenient on the plane P_W. Here, the assumption is that the room is parallelepipedic in shape.

Ceiling frame ($\mathcal{F}_C$) The ceiling plane P_C is parallel to the ground plane P_G and is separated by height **h** and located on the ceiling. Thus, the orientation of the ceiling frame ($\mathcal{F}_C$) is parallel to that of the ground frame ($\mathcal{F}_G$).

Wall frame ($\mathcal{F}_W$) Origin of the front wall frame O_W is fixed on the wall surface. Z-axis $\mathbf{z_W}$ is normal to the wall plane P_W. Axes $\mathbf{x_W}$ and $\mathbf{y_W}$ are mutually perpendicular and lie in plane P_W. Also, $\mathbf{z_W} = \mathbf{x_W} \times \mathbf{y_W}$. Thus, with respect to the frame $\mathcal{F}_E$, $\mathbf{z_W}$ is parallel to $\mathbf{x_E}$, $\mathbf{x_W}$ is parallel to $\mathbf{y_E}$ and $\mathbf{y_W}$ is parallel to $\mathbf{x_E}$ (Table 10.1).

Table 10.1 Description of frames

Frame ($\mathcal{F}$)	Position ($\mathcal{P}$)	Orientation ($\mathcal{O}$)
Environment ($\mathcal{F}_\mathcal{E}$)	At a convenient position on P_G	$\mathbf{z_E} \perp P_G$
		$\mathbf{y_E} = $ any of the two directions along $P_G \cap P_W$
		$\mathbf{x_E} = \mathbf{y_E} \times \mathbf{z_E}$
Ground ($\mathcal{F}_\mathcal{G}$)	At a convenient position on P_G	$\mathbf{z_G} \perp P_G$
		$\mathbf{y_G} = \mathbf{y_E}$
		$\mathbf{x_G} = \mathbf{x_E}$
Wall ($\mathcal{F}_\mathcal{W}$)	At a convenient position on P_W	$\mathbf{z_W} \perp P_W$
		$\mathbf{y_W} = \mathbf{h}, \mathbf{y_W} \epsilon P_W$
		$\mathbf{x_W} = \mathbf{w}, \mathbf{x_W} \epsilon P_W$
Ceiling ($\mathcal{F}_\mathcal{C}$)	At a convenient position on P_C	$\mathbf{z_C} \perp P_C$
		$\mathbf{y_C} = \mathbf{y_E}$
		$\mathbf{x_C} = \mathbf{x_E}, \mathbf{x_W} \epsilon P_W$
Robotic unit ($\mathcal{F}_\mathcal{R}$)	Center of the top face of the mobile base	$\mathbf{z_R} \perp P_G$
		$\mathbf{y_R} = \mathbf{y_G}$
		$\mathbf{x_R} = \mathbf{x_G}$
Support polygon ($\mathcal{F}_\mathcal{S}$)	Geometric centre of the support polygon	$\mathbf{z_S} \perp P_G$
		$\mathbf{y_S} = \mathbf{y_G}$
		$\mathbf{x_S} = \mathbf{x_G}$

Frame of the Robotic Unit ($\mathcal{F}_\mathcal{R}$) The frame of the robotic unit with origin O_R is attached to the centre of the top face of the mobile base. Axes $\mathbf{x_R}$ and $\mathbf{y_R}$ are directed along the length and the width of the mobile base and are parallel to plane P_G. Thus on a flat standard ground, orientation of axis $\mathbf{z_R}$ is parallel to axis $\mathbf{z_E}$.

Frame of the support polygon ($\mathcal{F}_\mathcal{S}$) The frame of the support polygon with origin O_S is attached to the centre of the support polygon of the mobile base. Axes $\mathbf{x_R}$ and $\mathbf{y_R}$ are directed along the length and the width of the mobile base and are parallel to axes $\mathbf{x_R}$ and $\mathbf{y_R}$ respectively. Naturally, orientation of axis $\mathbf{z_R}$ is parallel to axis $\mathbf{z_E}$.

Transformation between frames There exists a fixed transformation between environment frame ($\mathcal{F}_\mathcal{E}$) and frames representing components of the environment. i.e. wall frame ($\mathcal{F}_\mathcal{W}$), ground frame ($\mathcal{F}_\mathcal{G}$) and ceiling frame ($\mathcal{F}_\mathcal{C}$). These transformations are summarized in the Table 4.2. $\mathbf{R_k E}$ denotes a rotation matrix around axis $\mathbf{k_E}$ where, $k = x, y, z$ (Table 10.2).

Table 10.2 Transformation of frames w.r.t environment frame

Frame	Position w.r.t $\mathcal{F}_\mathcal{E}$	Orientation w.r.t $\mathcal{F}_\mathcal{E}$
Wall frame ($\mathcal{F}_w$)	$^E[o_{w_x} \; o_{w_y} \; o_{w_z}]$	$[\mathbf{R_{z_E}} \; (-\frac{\pi}{2}).\;\mathbf{R_{x_E}} \; (-\frac{\pi}{2})]$
Ground frame ($\mathcal{F}_\mathcal{G}$)	$^E[o_{g_x} \; o_{g_y} \; 0]$	
Ceiling frame ($\mathcal{F}_\mathcal{C}$)	$^E[o_{c_x} \; o_{c_y} \; o_{c_z}]$	$\mathbf{R_{y_E}} \; (-\pi)]$
Support polygon ($\mathcal{F}_\mathcal{S}$)	$^E[o_{s_x} \; o_{s_y} \; 0]$	$[\mathbf{R_{z_E}}]$
Robotic unit ($\mathcal{F}_\mathcal{R}$)	$^E[o_{r_x} \; o_{r_y} \; H_b.\hat{k}]$	$[\mathbf{R_{x_E}}]$

10.3 Modeling of Asbestos Removal Use Case

The process of asbestos removal involves positioning the mobile platform base in the cleaning environment at a suitable distance so as to access the maximum possible area at a given base position and be able to grind the surfaces with optimal grinding posture while maintaining the stability of the overall robotic unit.

Figure 10.14 shows robotic unit placed at a distance b from wall surface P_W. At this distance, the 3D workspace (W_A) of the robotic arm intersects with surface P_W for giving circle (C). The area of (C) is the area available for cleaning at a given base placement such that collision-free (arm-cleaning environment) continuous trajectories are feasible. However, since the robotic arm is mounted on a vertical slider Fig. 10.15, circle (C) can move along a vertical axis to sweep a surface with a geometric shape called 'stadium' (rectangle with semicircles on either of two opposite sides). Thus, even at a fixed base position, the workspace of the robotic arm is extended due to the presence of functional redundancy (P-joint).

10.3.1 Evaluation of Reaction Wrench

While realizing robotized grinding operation, it is inevitable to consider the difference in the geometry of the cleaning environment for precise modeling and simulation of the process. Moreover, the grinding operation generates a reaction wrench being applied to the end-effector. Since, the end-effector while cleaning different surfaces, takes different orientations, it is quite intuitive to conclude that the reaction wrenches acting on the robotic unit while cleaning these surfaces have different positions and orientations. Thus, the stability of the robotic unit is affected differently while performing the grinding operation of these surfaces.
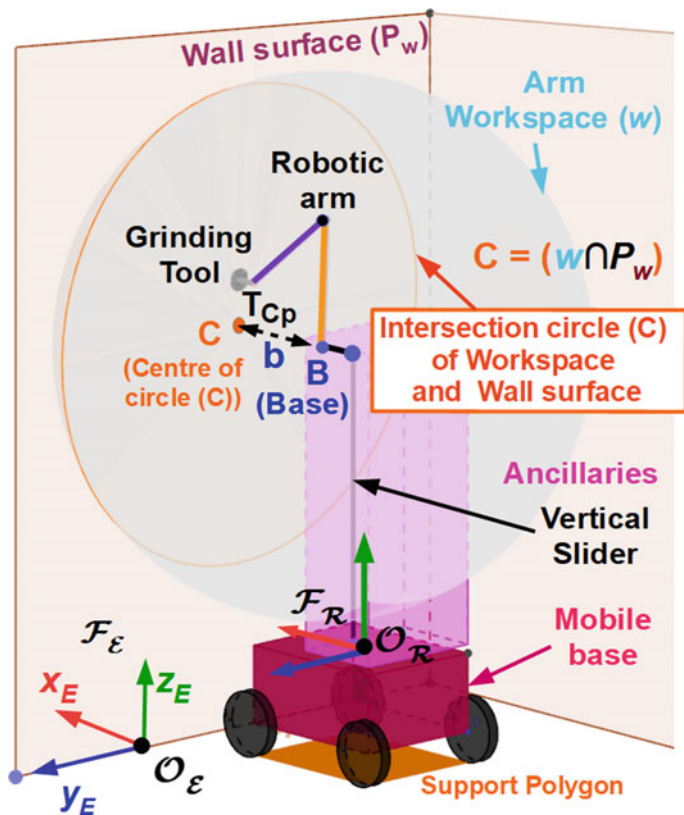
Fig. 10.14 Representation of workspace

10.3.2 Cleaning of Frontal Wall

Figure 10.16a shows reaction wrench being applied to the end-effector (tool) during the grinding operation while $\mathcal{F}_w : \{x_w, y_w, z_w\}$ indicates wall frame. Reaction wrench consists of normal reaction forces $[(\mathbf{F_{NZ}})_\mathbf{w}]$, tangential reaction forces $[(\mathbf{F_{TY}})_\mathbf{w}]$, $[(\mathbf{F_{TX}})_\mathbf{w}]$ and reaction torque $[(\mathbf{T_Z})_\mathbf{w}]$. Here, subscript '$w$' indicates that components of the reaction wrench are expressed in wall frame ($\mathcal{F}_w$). Normal and tangential reaction forces are responsible for producing moments that act on the robotic unit through the end-effector. These moments and the distances responsible for creating them are summarized in Table 10.3. Also, the effect of these forces on stability are identified.
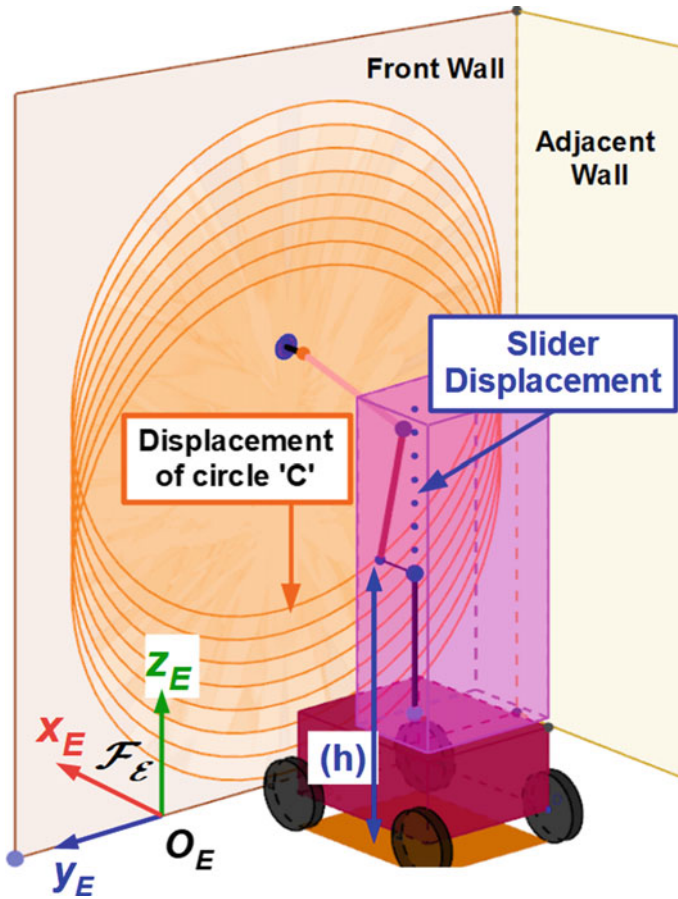
Fig. 10.15 Extension of workspace

Table 10.3 Generation of moments in wall scenario

Reaction force	Normal distance	Resulting moment	Probable effect on the robotic unit
$(\mathbf{F_{NZ}})_\mathbf{w}$	y_d	$\mathbf{M}_{z_S}$ (Moment around $\mathbf{z_S}$)	**Yaw** motion of the robotic unit
	z_d	$\mathbf{M}_{y_S}$ (Moment around $\mathbf{y_S}$)	**Pitch** motion affecting longitudinal stability
$(\mathbf{F_{TY}})_\mathbf{w}$	x_d	$\mathbf{M}_{z_S}$ (Moment around $\mathbf{z_S}$)	**Yaw** motion causing rotation of the platform
	z_d	$\mathbf{M}_{x_S}$ (Moment around $\mathbf{x_S}$)	**Roll** motion affecting lateral stability
$(\mathbf{F_{TX}})_\mathbf{w}$	x_d	$\mathbf{M}_{y_S}$ (Moment around $\mathbf{y_S}$)	**Pitch** motion affecting longitudinal stability
	y_d	$\mathbf{M}_{x_S}$ (Moments around $\mathbf{x_S}$)	**Roll** motion affecting lateral stability
		$(R)_w.\mathbf{x_S}$ (Reaction moment around $\mathbf{x_S}$)	Roll motion affecting lateral stability

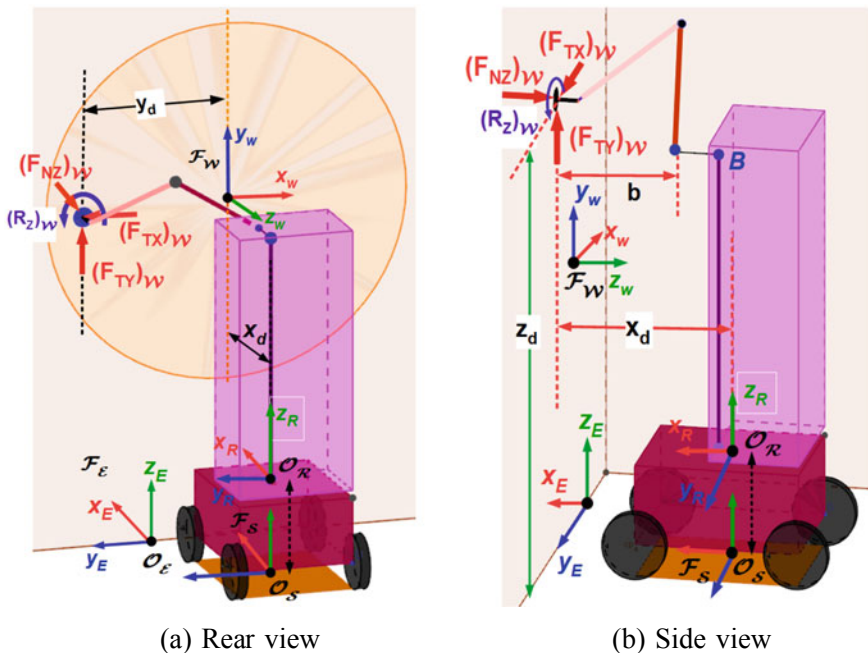(a) Rear view   (b) Side view

**Fig. 10.16** Forces and moments acting during wall cleaning scenario

Table 10.4 Generation of moments in ceiling cleaning scenario

Reaction component	Normal distance	Resulting moment	Probable effect on the robotic unit
$(\mathbf{F_{NZ}})_\mathbf{C}$	x_d	$\mathbf{M}_{y_S}$ (Motion around $\mathbf{y_S}$)	**Pitch** motion affecting longitudinal stability
	y_d	$\mathbf{M}_{x_S}$ (Moment around $\mathbf{x_S}$)	**Roll** motion affecting lateral stability
$(\mathbf{F_{TY}})_\mathbf{C}$	y_d	$\mathbf{M}_{z_S}$ (Moment around $\mathbf{z_S}$)	**Yaw** motion of the robotic unit
	z_d	$\mathbf{M}_{y_S}$ (Moment around $\mathbf{y_S}$)	**Pitch** motion affecting longitudinal stability
$(\mathbf{F_{TX}})_\mathbf{C}$	z_d	$\mathbf{M}_{x_S}$ (Moment around $\mathbf{x_S}$)	**Roll** moment affecting lateral stability
	x_d	$\mathbf{M}_{z_S}$ (Moment around $\mathbf{z_S}$)	**Yaw** motion of the robotic unit
		$(R_Z)_C.\mathbf{z_S}$ (Reaction moment around $\mathbf{z_S}$)	Yaw motion of the robotic unit

10.3.3 Cleaning of ceiling

For cleaning the ceiling portion of the environment, the directions of reaction forces differ from those during cleaning frontal walls. Reaction wrench consists of normal reaction force $[(\mathbf{F_{NZ}})_\mathbf{c}]$, tangential reaction forces $[(\mathbf{F_{NY}})_\mathbf{c}]$, $[(\mathbf{F_{NT}})_\mathbf{c}]$ (Fig. 10.17 and Table 10.4).

Fig. 10.17 Tool forces while cleaning ceiling
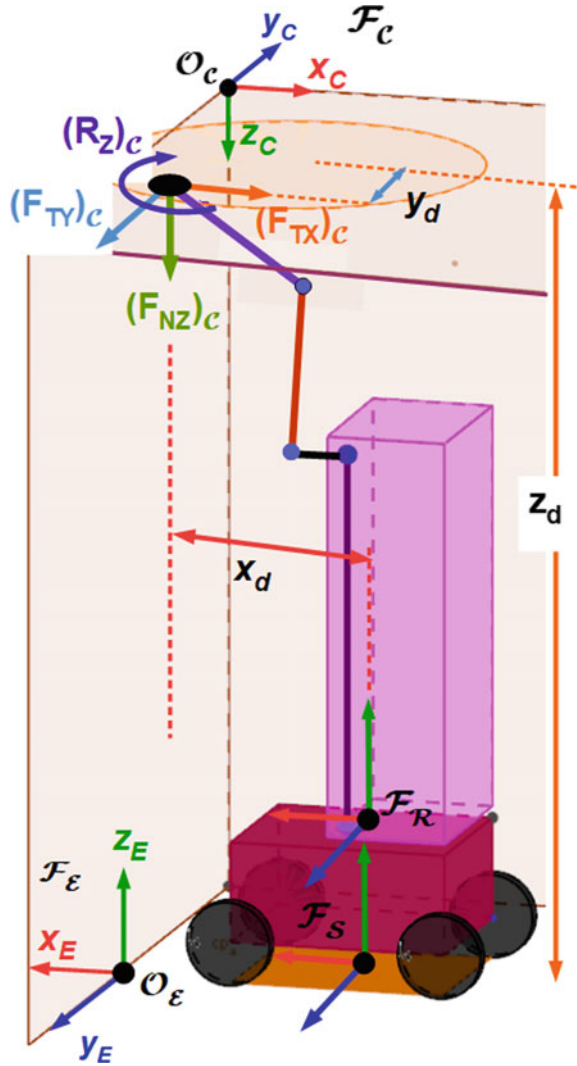
10.3.4 Cleaning of Ground

Ground cleaning is a scenario, as shown in Fig. 10.18. where the cleaning surface plane P_G and the plane defined by axes x_E-y_E of the environment frame are same. Reaction wrench consists of normal reaction force $[(F_{NZ})_G]$, tangential reaction forces $[(F_{TX})_G]$, $[(F_{TY})_G]$ and reaction torque $[(R_Z)_G]$. Since, tangential reaction forces lie in the plane of the support polygon, moments produced by these forces are zero in the ground plane. Thus, normal reaction force and reaction torque are the two entities that affect the stability of the robotic unit (Table 10.5).
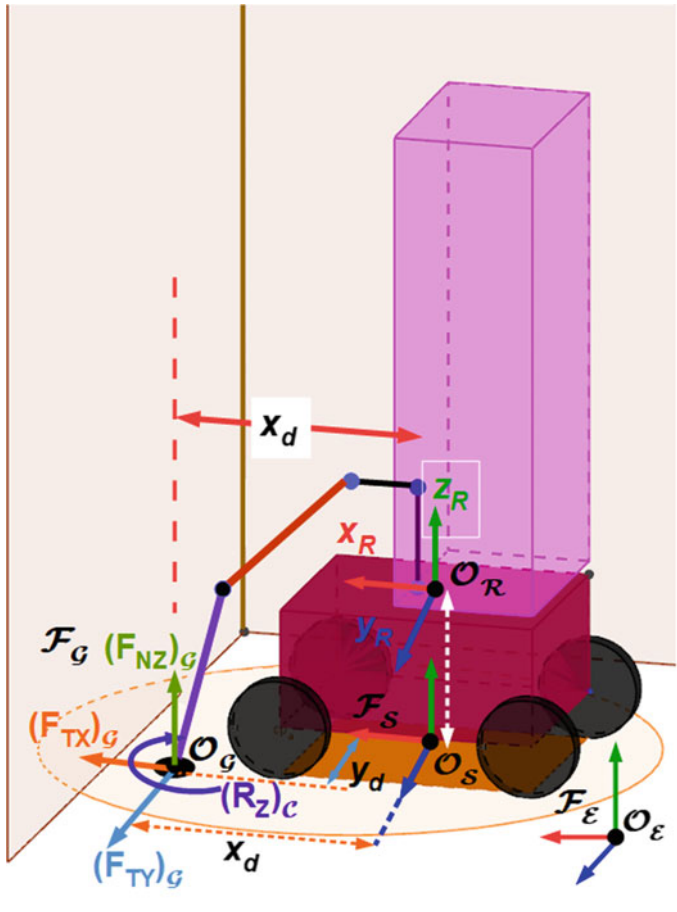
Fig. 10.18 Tool forces while cleaning ground

Table 10.5 Generation of moments in ground cleaning scenario

Reaction force	Normal distance	Resulting moment	Effect on the robotic unit
$(\mathbf{F_{NZ}})_\mathbf{G}.(\mathbf{z}_S)$	z_d	$\mathbf{M}_{y_S}$ (Moment around $\mathbf{y_S}$)	Pitch moment affecting longitudinal stability
	y_d	$\mathbf{M}_{x_S}$ (Moment around $\mathbf{x_S}$)	Roll motion affecting lateral stability
		$(\mathbf{R_z})_\mathbf{G}.\mathbf{z_S}$ (Reaction moment around $\mathbf{z_S}$)	Yaw motion of the platform

10.3.5 Stability Criteria Based on Zero Moment Point

Issues regarding the stability of the robotic unit during grinding operation are already discussed in previous sections. In order to ensure safe and stable operation, a suitable stability margin must be defined. For a dynamically operating system, ZMP is widely used in the field of biped locomotion. ZMP is defined as a point on the ground at which the net moment of the inertial forces and the gravity forces has no component along the horizontal axes [23]. The two components of ZMP are determined by:

$$x_{zmp} = \frac{\sum_{i=1}^{n} m_i(\ddot{z}_i + g)x_i - \sum_{i=1}^{n}(m_i\ddot{x}_i)z_i - \sum_{i=1}^{n}(\mathcal{L}_y)_i}{\sum_{i=1}^{n} m_i(\ddot{z}_i + g)} \tag{10.13a}$$

$$y_{zmp} = \frac{\sum_{i=1}^{n} m_i(\ddot{z}_i + g)y_i - \sum_{i=1}^{n}(m_i\ddot{y}_i)z_i - \sum_{i=1}^{n}(\mathcal{L}_x)_i}{\sum_{i=1}^{n} m_i(\ddot{z}_i + g)} \tag{10.13b}$$

where, i indicates number of rigid bodies, (x_i, y_i, z_i) indicate coordinates of the CoM of the ith body and $(\mathcal{L}_x, \mathcal{L}_y)$ indicate the components of angular momentum derivatives, where, $\mathcal{L}_i = I_i\dot{\omega} + \omega_i \times I_i\omega_i$; ω_i is the angular velocity of link i and I_i is its inertia matrix.

From the definition of ZMP, we see that each term in the numerator represents a moment acting on the system. Thus, to integrate grinding reaction forces in ZMP, moments produced by normal and tangential reaction forces must be taken into account. These moments are already identified in the Sect. 10.3.1.

$$x_{zmp} = \frac{\sum_{i=1}^{n} m_i(\ddot{z}_i + g)x_i - \sum_{i=1}^{n}(m_i\ddot{x}_i)z_i - \sum_{i=1}^{n}(\mathcal{L}_y)_i - \mathbf{M}_{y_S}}{\sum_{i=1}^{n} m_i(\ddot{z}_i + g)} \tag{10.14a}$$

$$y_{zmp} = \frac{\sum_{i=1}^{n} m_i(\ddot{z}_i + g)y_i - \sum_{i=1}^{n}(m_i\ddot{y}_i)z_i - \sum_{i=1}^{n}(\mathcal{L}_x)_i - \mathbf{M}_{x_S}}{\sum_{i=1}^{n} m_i(\ddot{z}_i + g)} \tag{10.14b}$$
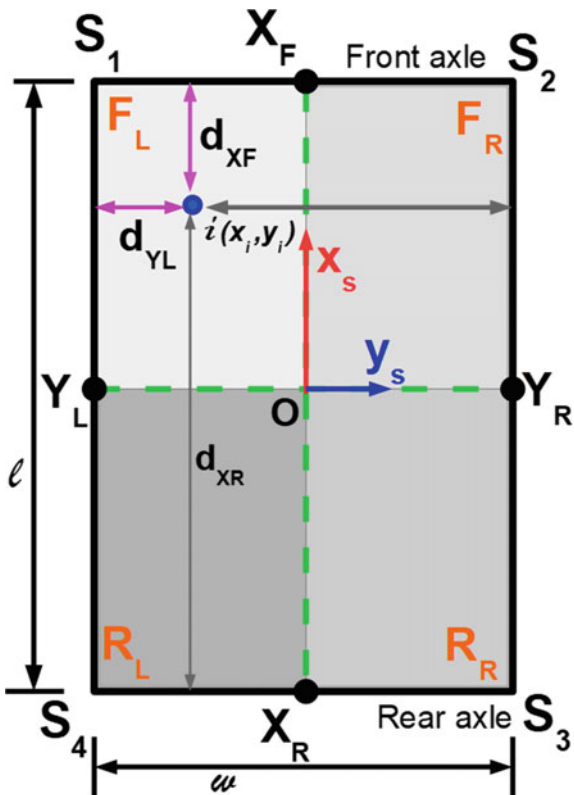
Stability Index

In our case, the mobile base has rectangular support polygon $S_1S_2S_3S_4$ of dimensions $(l \times w)$ mm with lateral and longitudinal axes Y_LY_R and X_FX_R respectively (see Fig. 10.19). The polygon is divided in four quadrants namely, front-left (F_L), front-right (F_R), rear-left (R_R) and rear-right (R_R). Longitudinal (S_{long}) and lateral (S_{lat}) percentage stability of point 'i' having ZMP coordinates (x_i, y_i) is calculated as,

$$S_{long} = \left(\frac{min(d_{XF}, d_{XR})}{0.5 \times l}\right) \times 100, \quad S_{lat} = \left(\frac{min(d_{YR}, d_{YL})}{0.5 \times w}\right) \times 100 \tag{10.15}$$

where, $d_{XF} = \left|\frac{l}{2} - x_{zmp}\right|, d_{XR} = \left|\frac{l}{2} + x_{zmp}\right|, d_{YL} = \left|\frac{w}{2} - y_{zmp}\right|, d_{YR} = \left|\frac{w}{2} + y_{zmp}\right|.$

Fig. 10.19 Notations for stability in the support polygon

10.4 Numerical Evaluation of Stability

An algorithm to carry out a numerical evaluation of stability is implemented using MATLAB computing software (Fig. 10.20). The main objective of developing numerical method is to exploit the computational efficiency of MATLAB script execution, which is much higher than that of the co-simulation with a black-box dynamic model in ADAMS. Numerical simulation is a fast way to simulate the simplified dynamics of the robot as it simplifies the process of simulation by avoiding repetitive steps like modifying the initial posture of the arm for different trajectories.

   A general approach adapted in defining the algorithm is explained below:

- *Cartesian trajectory input*: Targeted operational surfaces in construction applications can be 3-dimensional in nature (curved walls, ceiling or ground). However, in the chapter, the focus is limited to non-curved surfaces. Thus, 2-D Cartesian trajectories are defined while performing simulations. Cartesian poses of the end-effector frame corresponding to trajectory coordinates serves as an input to the algorithm.
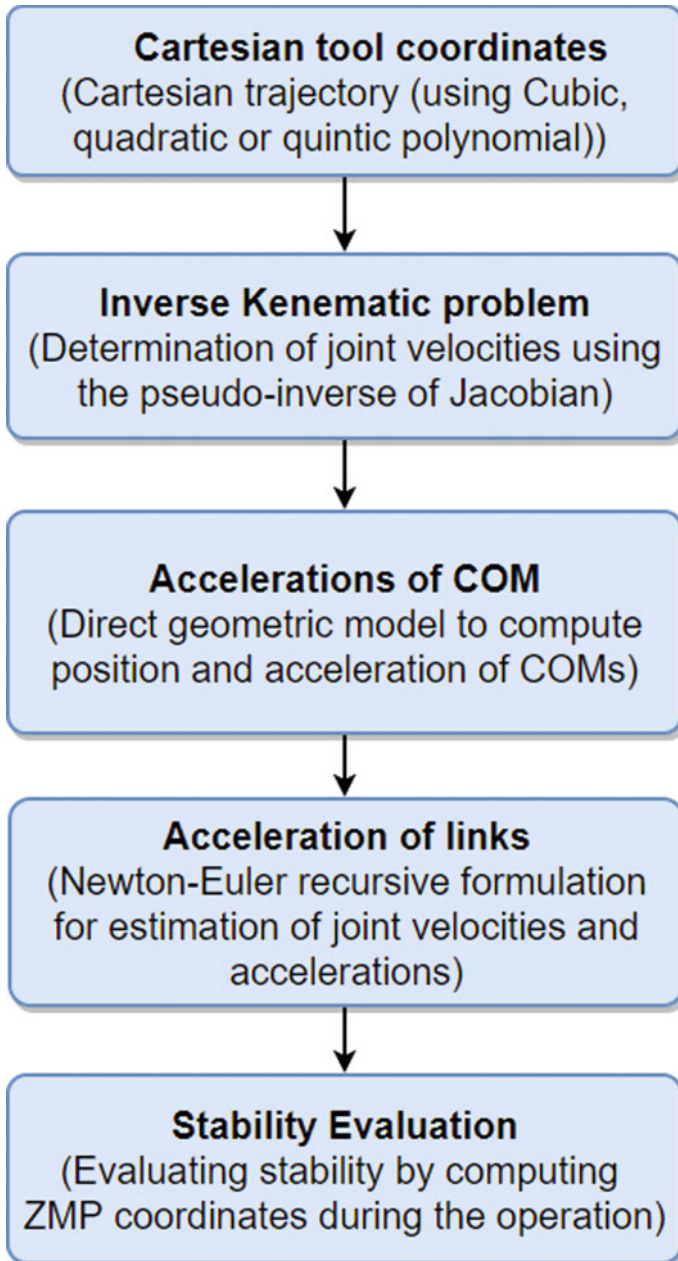
Fig. 10.20 Workflow of numerical evaluation of stability based on ZMP

Table 10.6 Features of ADAMS and MATLAB

ADAMS	MATLAB/Simulink
–Modeling of Mechanical system	
–Importing CAD parts (e.g. CATIA)	–Designing control architecture
–Parameterization of design	using block diagrams
–Modeling contacts (with friction)	Predefined blocks
–Applying external force	–Defining MATLAB function blocks
–Defining input-output variables	within control model
control variables	–Data logging and processing
–Robust dynamic solver	
–Measuring output variables	

- *IKS*: Inverse kinematics solution is needed to generate arm motion. Since, arm is kinematically redundant, IKS is determined using the redundancy resolution method that uses pseudo-inverse of the kinematic Jacobian matrix.
- *Recursive computation of link accelerations*: Angular velocities and accelerations of moving links contribute to generating dynamic effects on the robotic unit. Newton-Euler recursive algorithm is used to compute these entities.
- *Stability Evaluation*: Zero moment point for the instantaneous dynamic state of the robotic unit is computed using Eqs. 10.14a and 10.14b. Stability is then evaluated as per Eq. 10.15.

For evaluating stability during a continuous trajectory, the algorithm runs in loops defined by end positions of the trajectory.

10.5 Stability Evaluation Using Co-Simulation

Cooperation of dynamic modeling and simulation tool—ADAMS with the computing software MATLAB is a known methodology in the robotics research community. In [1], the importance of co-simulation is highlighted for the robotics domain by simulating a 2-link planar robot. Several other notable works are also mentioned. Co-simulation combines features of both software and provides a robust and efficient tool for dynamic system analysis (Fig. 10.21 and Table 10.6).

10.5.1 Development of Cosimulation Model

It is a multi-body dynamic model positioned inside cleaning environment consisting of ground, ceiling and frontal wall (Fig. 10.22). Peculiarities of the model are enlisted below:
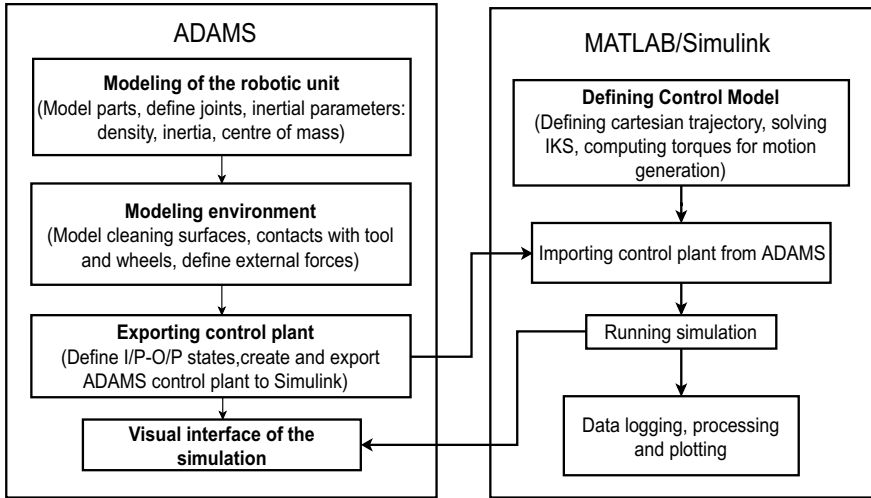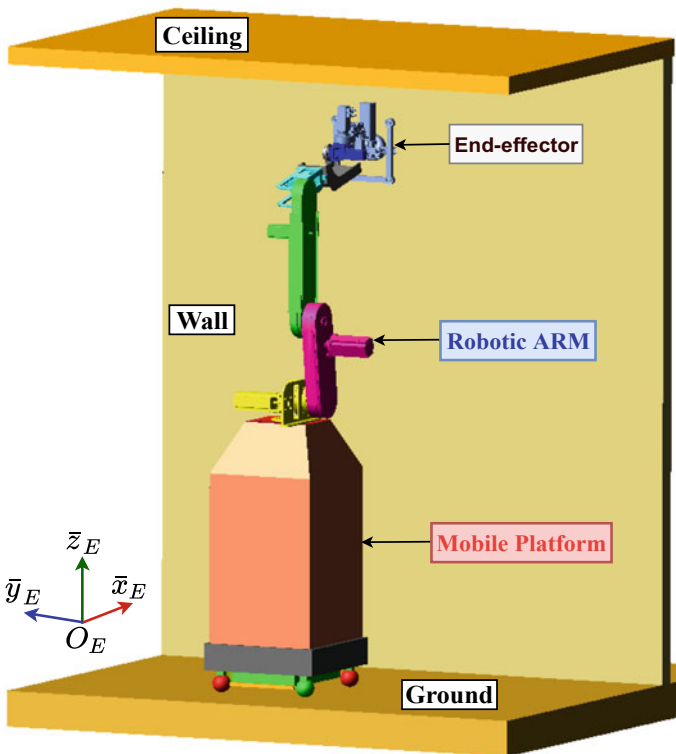
Fig. 10.21 Flow-chart of ADAMS-Matlab co-simulation

Fig. 10.22 Multibody dynamic model of the robotic unit version-2 in ADAMS
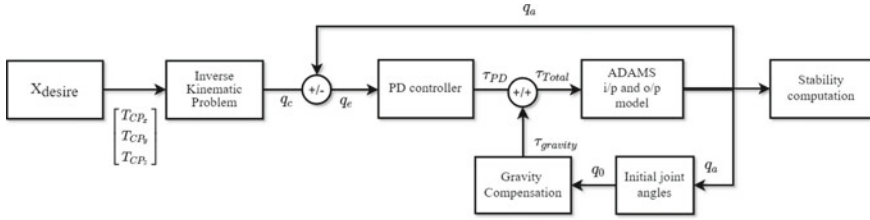
Fig. 10.23 ADAMS-simulink control model for stability evaluation

- *Part modeling*: Simple geometric shapes like sphere, cylinder, cuboid etc. are used to create a multi-body model of the robotic unit. These are solid rigid bodies that can mutually interact to generate displacement, reaction forces etc. Construction of robotic arm is performed by importing parts from CATIA as .stl files.
- *Parameterization*: It can be achieved through design variables (DV). They are used as an input (length, width etc.) to the geometric shapes. By changing the value assigned to the DVs, geometries can be quickly modified or re-positioned in the environment.
- *Joints/motion constriants*: Prismatic and revolute joints are added to create suitable joint angles between bodies. Static components are connected using fixed joints. Joints can also be parameterized to change the posture of the arm (or individual link). This is helpful in achieving suitable initial posture during co-simulation.
- *Contact modeling*: Contacts between the grinding tool and cleaning surface is created to generate reaction forces. Similarly, contacts between wheels of the mobile manipulator and ground surface are created to restrict the motion of the robotic unit in the plane and record ground reaction forces. Contact feature in ADAMS allows selecting coefficients of static and dynamic friction.
- *Inertia parameters*: Values of mass, inertia matrices and positions of CoM are determined through CAD models and are added to the components (Fig. 10.23).

q_c :	command joint position.
q_a :	actual joint position.
q_e :	$(q_c - q_a)$ i.e. error in the joint position.
τ_{PD}	torque generated by PD-controller.
$\tau_{Gravity}$:	torque input for gravity compensation.
τ_{Total} :	total torque input for joint.
T_{CP_x} :	x-coordinate of the tool.
T_{CP_y} :	y-coordinate of the tool.
T_{CP_z} :	z-coordinate of the tool.
X_{desire} :	desired Cartesian coordinates of tool centre point.

For the sake of simplification, the following assumptions are made while developing the model:

1. the ground surface is even.
2. the center of mass (CoM) of the platform coincides with its center of geometry.

Table 10.7 MDH parameters

(i)	σ	θ	d	α	r
1	1	0	0	0	r_1^*
2	0	q_2	0	0	0.1
3	0	q_3	0.1	$\frac{pi}{2}$	0.9
4	0	q_4	0.6	0	0
5	0	q_5	0.6	$-\frac{pi}{2}$	0
6	0	q_6	0.13	$-\frac{pi}{2}$	0.13
7	0	q_7	0	0	0

$*r_1 = h = (0.5, 1.8)\,m$

3. all wheels are always in contact with the ground. i.e., no slippage of the wheels occurs.
4. the onboard manipulator is rigidly connected with the platform, and the links of the onboard manipulator are rigid.

10.5.2 Validation of Stability Evaluation Approaches

In this section, the stability of the version-1 prototype is demonstrated while performing a vertical zig-zag trajectory. MDH model of the P-6R arm architecture mounted on the robotic unit is presented in Table 10.7 and Fig. 10.24.

Figure 10.25 represents the path traversed by the tool. It traverses two trajectories—SE_1 and SE_2. Figure 10.26 shows front half of the support polygon. Axis AB defines the front axle. The black dotted lines are 25% stability lines. The figure shows variation of ZMP obtained for the cleaning trajectory.

The black line shows ZMP trace calculated using numerical approach while the pink line traces ZMP from co-simulation. The approximate overlapping of the two traces validates the numerical approach.

10.6 Conclusion

This chapter detailed the dynamic modeling of the robotic unit for stability evaluation. Initially, the robot-environment interaction model was presented to highlight the need for developing the dynamic model. Thereafter, the cleaning environment and the robotic unit were described through representative frames. This representation provided a base for developing the numerical model. Using Geogebra illustrations, the process of asbestos removal was analyzed to identify reaction wrench acting on the robotic unit during different cleaning scenarios namely wall, ceiling and ground.
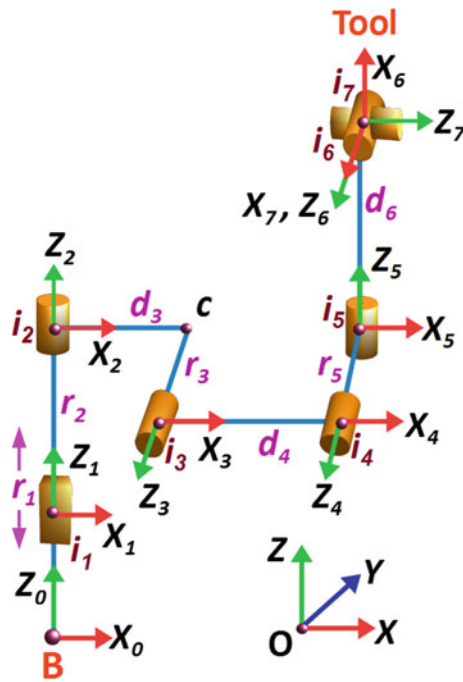
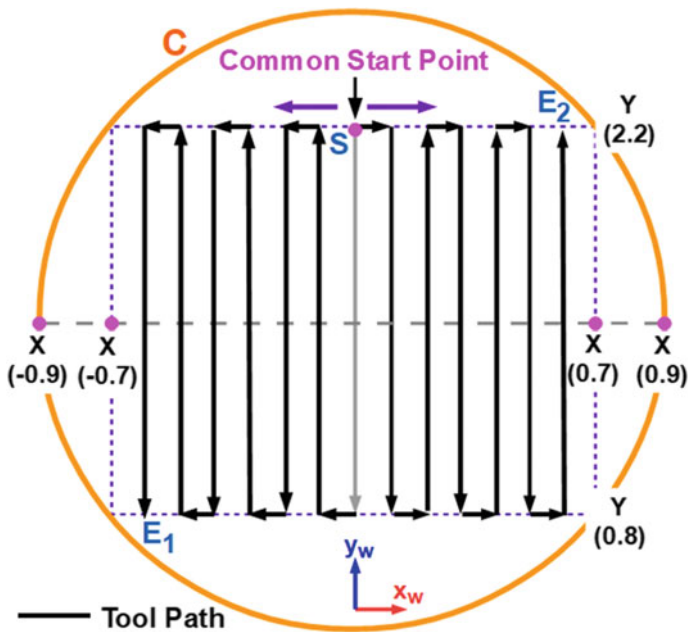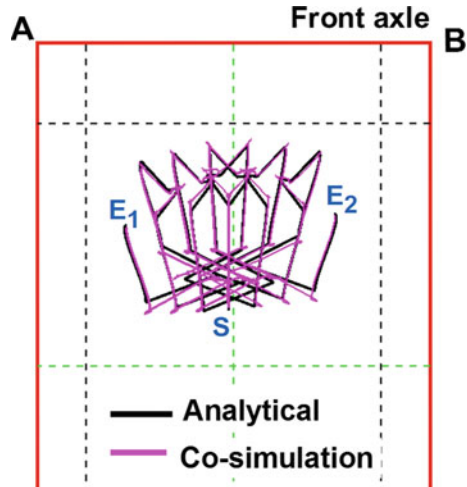**Fig. 10.24** Visualization of the P-6R architecture

Fig. 10.25 Path traced by tool on the wall

Fig. 10.26 ZMP estimation
through analytical and
co-simulation

Further, the approach for the numerical evaluation of dynamic stability based on the zero moment point (ZMP) was elaborated. The steps of this approach are, kinematic modeling of the robotic unit, trajectory generation and solving the inverse kinematic problem have been explained in detail. The method of co-simulation for evaluating stability was developed so as to validate the results to be obtained by the numerical approach. A multi-body dynamic model of the robotic unit was developed in MSC ADAMS software which provides information on the behavior of the system (joint velocities, accelerations, etc.). Control commands of this model were fed in the Simulink environment.

References

1. Angel, L., Pèrez, M.P., Diaz-Quintero, C., Mendoza, C.: ADAMS/MATLAB co-simulation: dynamic systems analysis and control tool. Appl. Mech. Mat. **232**, 527–531 (2012)
2. Armada, E.G., Estremera, J., Santos, P.G.D.: A classification of stability margins for walking robots. In: Proceedings of International Symposium on Climbing Walking Robots, pp. 799–808 (2002). http://digital.csic.es/handle/10261/8031
3. Bots2ReC: Home|Bots2ReC (2016). https://www.bots2rec.eu. Accessed on 25 Oct 2018
4. Davidson, J.K., Schweitzer, G.: A mechanics-based computer algorithm for displaying the margin of static stability in four-legged vehicles. J. Mech. Des. Trans. ASME **112**(4), 480–487 (1990)
5. Diaz-Calderon, A., Kelly, A.: On-line stability margin and attitude estimation for dynamic articulating mobile robots. Int. J. Robot. Res. **24**, 1–41 (2005)
6. Ding, X., Liu, Y., Hou, J., Ma, Q.: Online dynamic tip-over avoidance for a wheeled mobile manipulator with an improved tip-over moment stability criterion. IEEE Access **7**, 67632–67645 (2019)
7. Garcia, E., De Santos, P.G.: An improved energy stability margin for walking machines subject to dynamic effects, vol. 23 (2005)

8. Ghasempoor, A., Sepehri, N.: Measure of machine stability for moving base manipulators. In: Proceedings—IEEE International Conference on Robotics and Automation, vol. 3, pp. 2249–2254 (1995)
9. Hirose, S., Tsukagoshi, H., Yoneda, K.: Normalized energy stability margin and its contour of walking vehicles on rough terrain. In: Proceedings 2001 ICRA. IEEE International Conference on Robotics and Automation (Cat. No.01CH37164), vol. 1, pp. 181–186 (2001)
10. Lee, J.H., Park, J.B., Lee, B.H.: Turnover prevention of a mobile robot on uneven terrain using the concept of stability space. Robotica **27**(5), 641–652 (2009)
11. Lin, B.-S., Song, S.-M.: Dynamic modeling, stability and energy efficiency of a quadruped walking machine. In: IEEE International Conference on Robotics and Automation, vol. 18(11), pp. 367–373 (1993)
12. Mahdi, A., Nestinger, S.S.: Foot force criterion for robot stability, pp. 23–26 (2012)
13. McGhee, R., Frank, A.: On the stability properties of quadruped creeping gaits. Math. Biosci. **3**, 331–351 (1968)
14. Mcghee, R.B., Iswandhi, G.I.: Adaptive locomotion of a multilegged robot over rough terrain. IEEE Trans. Syst. Man Cybern. **9**(4), 176–182 (1979)
15. Messuri, D.A., Klein, C.A.: Automatic body regulation for maintaining stability of a legged vehicle during rough-terrain locomotion. IEEE J. Robot. Autom. **1**(3), 132–141 (1985)
16. Moosavian, S., Alipour, K.: Moment-height tip-over measure for stability analysis of mobile robotic systems. In: 2006 IEEE/RSJ International Conference on Intelligent Robots and Systems, pp. 5546–5551 (2006)
17. Moosavian, S.A.A., Alipour, K.: On the dynamic tip—over stability of wheeled mobile manipulators. Int. J. Robot. Autom. **22**(4) (2007)
18. Papadopoulos, E., Poulakakis, J.: Planning and model-based control for mobile manipulators. In: 2000 IEEE/RSJ International Conference on Intelligent Robots and Systems, 2000. (IROS 2000). Proceedings, vol. 3, pp. 1810–1815. IEEE (2000)
19. Papadopoulus, E., Rey, D.: A new measure of tipover stability margin for mobile manipulators. In: Proceedings of the IEEE International Conference on Robotics and Automation, Minneapolis, MN, pp. 3111–3116 (1996)
20. Roan, P.R., Burmeister, A., Rahimi, A., Holz, K., Hooper, D.: Real-world validation of three tipover algorithms for mobile robots. In: Proceedings—IEEE International Conference on Robotics and Automation, pp. 4431–4436 (2010)
21. Sreenivasan, W.B.H.: Stability and tractson control of an actively actuated micro-rover. J. Robot. Syst. **11**(6), 487–507 (1994)
22. Sugano, S., Huang, Q., Kato, I.: Stability criteria in controlling mobile robotic systems. In: Proceedings of 1993 IEEE/RSJ International Conference on Intelligent Robots and Systems (IROS '93), (C), pp. 832–838 (1993)
23. Vukobratovic, M., Juricic, D.: Contribution to the synthesis of biped gait. In: Proceedings of IFAC Symposium on Technical and Biological Problems on Control, Erevan, USSR (1971)
24. Yoneda, K., Hirose, S.: Stability criterion of integrated locomotion an manipulation. In: Proceedings IROS 96, pp. 870–876 (1996)